

Chapter 2

On the Aggregation and Extrapolation of Uncertainty from Component to System Level Models

Angel Urbina, Richard G. Hills, and Adam C. Hetzler

Abstract The use of computational models to simulate the behavior of complex mechanical systems is ubiquitous in many high consequence applications such as aerospace systems. Results from these simulations are being used, among other things, to inform decisions regarding system reliability and margin assessment. In order to properly support these decisions, uncertainty needs to be accounted for. To this end, it is necessary to identify, quantify and propagate different sources of uncertainty as they relate to these modeling efforts. Some sources of uncertainty arise from the following: (1) modeling assumptions and approximations, (2) solution convergence, (3) differences between model predictions and experiments, (4) physical variability, (5) the coupling of various components and (6) and unknown unknowns. An additional aspect of the problem is the limited information available at the full system level in the application space. This is offset, in some instances, by information on individual components at testable conditions. In this paper, we focus on the quantification of uncertainty due to differences in model prediction and experiments, and present a technique to aggregate and propagate uncertainty from the component level to the full system in the applications space. A numerical example based on a structural dynamics application is used to demonstrate the technique.

Keywords Aggregation • Extrapolation • Uncertainty propagation

Nomenclature

F	Force
f_n	Frequency of interest
m	Mass of test article
ζ	Instantaneous damping

2.1 Introduction

The reliability of high consequence systems, such as aerospace components, has been traditionally established by testing individual systems and verifying their performance is within some acceptable limits. Although full scale testing is currently not feasible for some systems under actual use environments, some limited testing is often available for components, subsystems (i.e. groups of components) and a very limited number of tests of the full system in other use environments. Modeling and simulation attempt to fill the gap left by the lack of full scale testing for the actual use environments. Because component level data are usually cheaper and easier to obtain relative to the system data, it is advantageous to have the ability to build individual models of the component and/or subsystems using available data and incorporate them into a system level model. This leads to a hierarchical approach to building system level models and consequently the uncertainty in the system model is a function of the component level data and of the knowledge not captured in the component or subsystem level data.

A. Urbina (✉) • R.G. Hills • A.C. Hetzler
Sandia National Laboratories, P.O. Box 5800, MS 0828, Albuquerque, NM 87185, USA
e-mail: aurbina@sandia.gov

Furthermore, because tests cannot be performed for many actual use environments, the model is required to extrapolate beyond the data it was developed from. To establish confidence in an extrapolated model prediction, sources of uncertainty must be identified, quantified and propagated to the response quantity of interest at the system model.

Recently, there has been an emphasis on developing models of components using first principles, calibrating them from simple exploratory experiments, validating them relative to a different set of experiments and then using them within a more complex model. For example, one could investigate the behavior of mechanical joint using simple experiments, develop a model that explains some phenomenon of interest, validate its performance on a different environment and use it as part of a larger system. What was described above is defined as a hierarchical approach to building a system level model. It is basically a construction of a complex system model by using a building block approach that incorporates simpler component based models and couples them together. This hierarchical model building approach was described in several published papers [1, 2]. To quantify uncertainty, multiple tests of these components should be available from which an estimate of the variability in the components could be obtained. Adding to the uncertainty is the possibility that the interactions of the various components was never tested, thus no information on the coupling of components will be available. In addition, interactions of components could have been tested at excitation levels that are not comparable to those of the full system, thus giving rise to another source of uncertainty.

In this paper, we focus on the quantification of uncertainty due to differences in model prediction and experiments, and present a technique to aggregate and propagate these sources from the component level to the applications space. A numerical example based on a structural dynamics application is used to demonstrate the technique.

2.2 Example Problem Description

The example problem has the following features:

- It is a multi-component problem which involves a mechanical joint which provides an energy dissipating mechanism.
- It is a multi-level problem where the phenomena observed at the lowest level is assumed to be present at subsequent levels, i.e. damping in the joints is assumed similar at all levels. This might turn out to be an incorrect assumption.
- Experimental data consists of repeated tests on several, nominally identical hardware systems. These are intended to quantify the variability inherent in a physical system.
- Simple finite element models are built and calibrated to simulate a particular behavior of the physical hardware. The model parameters have been calibrated from simple, discovery experiments aimed at isolating the particular physical phenomenon that the model is trying to represent. Parametric uncertainty is explored in this paper.

The levels of complexity in this problem are defined as follows:

Level 1

- Dumbbell configuration: 45 joint samples tested with an impulse type excitation.

Level 2

- Three leg configuration (wavelet input): 27 joint samples tested using a wavelet-type.

Application level

- Three leg configuration (shock input): 27 joint samples tested using a shock-type input excitation.

In all levels, acceleration time histories were recorded and energy dissipation was calculated for each experiment and for each model prediction. The particular details of each level are described in the following sections.

2.2.1 Dumbbell Configuration (Level 1)

This configuration has two, 30 lb masses bolted at the ends of a single leg (or joint) creating a “dumbbell” looking hardware. This is shown in Fig. 2.1. This configuration is supported by bungee cords to simulate a free-free environment and it is subjected to an impulse excitation, on one of the end masses, provided by an instrumented hammer. The acceleration response of the dumbbell on the side opposite to the excitation is recorded and also shown in Fig. 2.1. From this response, the free decay time history of the response is obtained and used to estimate the energy dissipation of the system at a particular force

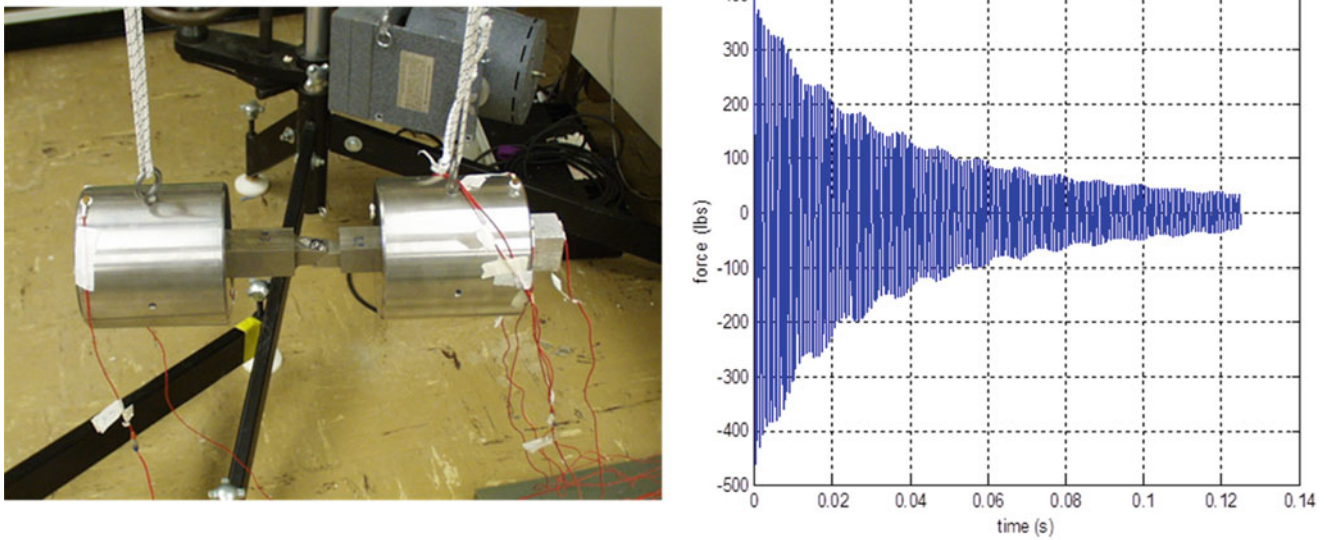


Fig. 2.1 Level 1 test configuration (left picture) and example transient ring down to hammer input (right figure)

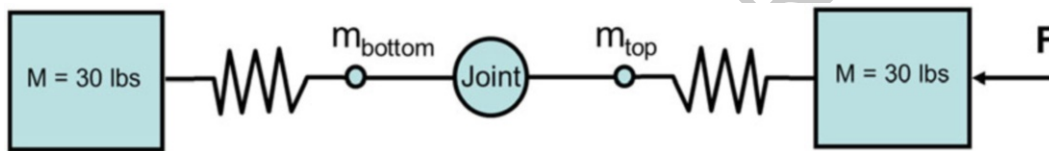


Fig. 2.2 Schematic of finite element model for test hardware

level. A total of 45 experiments were conducted to characterize unit-to-unit and test-to-test variability. A simplified finite element model of the dumbbell hardware is schematically represented in Fig. 2.2. This includes an energy dissipation model denoted as “Joint”. Further details on this model are given later in the paper.

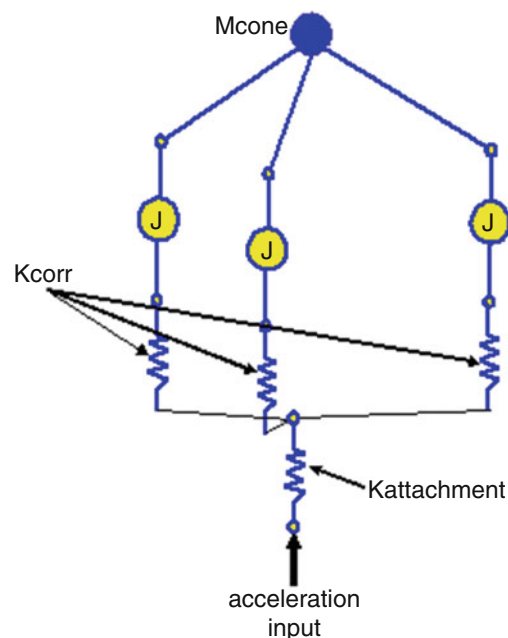
2.2.2 Three-Leg Configuration (Level 2 and Application Space)

The experimental system at these levels is a truncated conic shell supported on legs at three approximately symmetric locations. The support structure beneath the legs is a cylindrical shell—relatively thin on its top, and transitioning into a thicker section. The conic shell is attached to the support structure via three screws, each of which passes through a hole in a thin, flat plate at the top of a leg. Three nominally identical replicates of the conic shell were fabricated, along with three nominally identical support structures. A schematic of this is shown in Fig. 2.3. The nine combinations of shells and support structures were tested with two distinct environments: (1) a wavelet type excitation and (2) a shock type excitation. The excitations are also shown in Fig. 2.3. Each shell-base combination was assembled-disassembled-reassembled three times, and tested each time. The average acceleration structural responses at the tops of the shells are shown in Fig. 2.4 for the shock environment. There are 27 time histories—nine structures times three tests each.

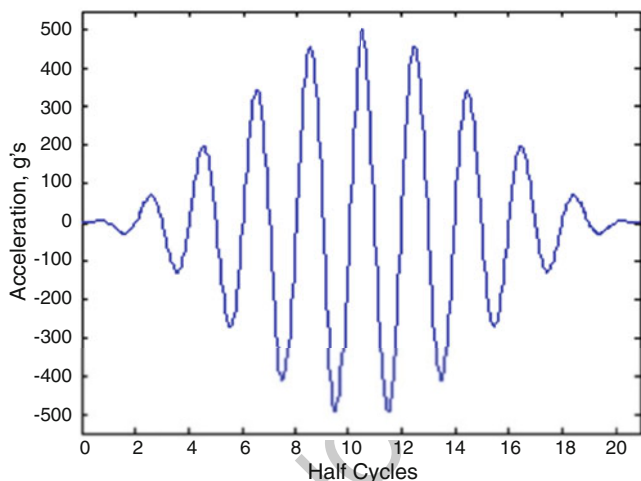
The finite element model for the physical system used in the current analysis is the lumped-mass representation shown in Fig. 2.3. The energy dissipation mechanisms are noted as J in the figure. Predictions, with uncertainty, of the response under a shock environment are the focus of our paper.

2.2.3 Energy Dissipation Model: Iwan Model

The element critical in this study is a nonlinear energy dissipating mechanism (denoted “Joint” in Fig. 2.2 and J in Fig. 2.3), and is modeled using the framework of the so-called Iwan element. The element is described in [3]. The four parameters of



Wavelet excitation



Shock excitation

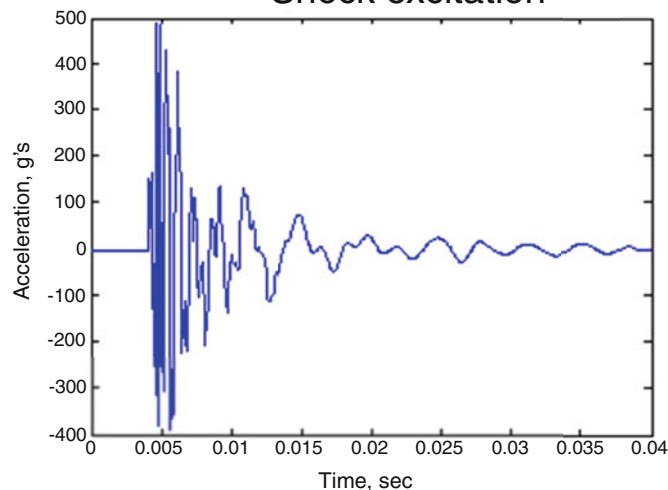
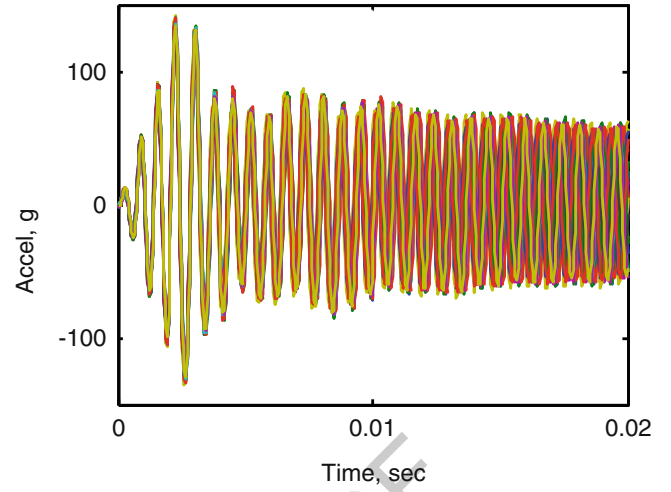


Fig. 2.3 Schematic representation of tested system (*top figure*) and the inputs used to excite it (*bottom figures*)

the nonlinear, Iwan spring element were identified based on experiments in which individual joint-simulators were excited sinusoidally. Multiple systems were tested, and they are stochastic, therefore, the parameters of the Iwan model are described in a probabilistic framework. An approach to estimating the parameters of the Iwan model and their uncertainty is described in [4]. Because the geometry and boundary conditions of the system used to identify Iwan model parameters differ from the geometry and boundary conditions of the three-legged system, correction stiffness, K_{corr} and attachment stiffness, $K_{attachment}$ needed to be added to the lumped mass model to render its predictions accurate. The attachment stiffness was calibrated by matching the axial frequency of a monolithic structure and assuming that the stiffness of the cone was essentially rigid when compared to the rest of the structure. The correction stiffness was calculated and inserted into the lumped-mass model. Analysis of this model was done in Salinas, a primarily linear structural dynamics analysis code written at Sandia [5].

Fig. 2.4 Acceleration responses at the top of the test structures for the shock excitation



Energy dissipation per cycle from transient responses

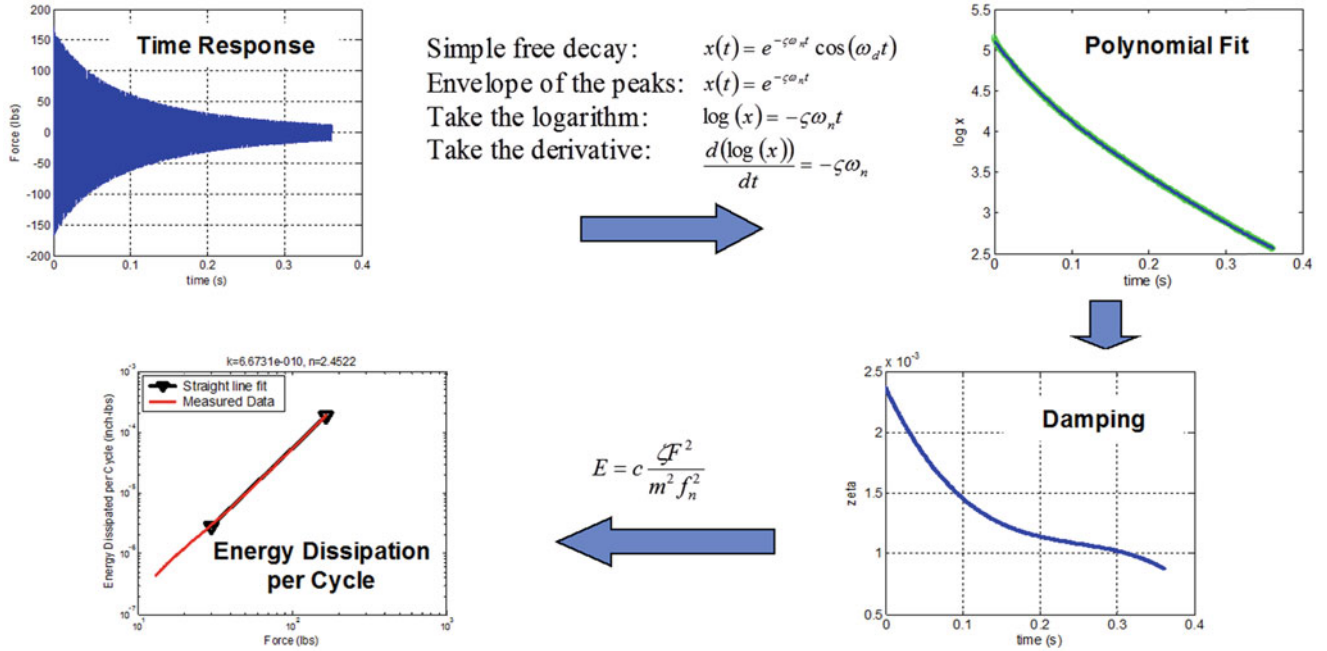


Fig. 2.5 Calculation of the energy dissipation quantity

2.2.4 Quantity of Interest: Energy Dissipated (E_d)

104

The energy dissipation from the transient ring down experiment is chosen as the quantity of interest to use in this study. The process to calculate this metric is shown in Fig. 2.5 and more details can be found in [6]:

106

2.3 Uncertainty Quantification, Aggregation and Propagation

107

2.3.1 Training Data and Partial Least Squares Regression

108

The goal of this research is to develop a correction to model based predictions of energy dissipation for the three-leg configuration under shock loading (application level), given the model predictions and experimental results for the dumbbell

110

(Level 1) and three-leg wavelet test (Level 2) configurations. The Partial Least Squares Regression (PLS) based approach developed by Hills [7] is used to develop a linear relationship between differences in experiment and model predictions throughout a validation hierarchy, and a correction to a model prediction for the target application. Using the probabilistic model of the four parameters of the Iwan model, we generate 20 sets of the four parameters and used in the models of the dumbbell and three leg configuration. Each model is run using Salinas and there are a total of 60 model runs. Acceleration time history responses were obtained and subsequently post-processed, using the procedure shown in Fig. 2.5, to obtain an estimate of the energy dissipation for each run. The resulting data is referred to as the training sets and will be used to develop this regression. To perform this regression, the training sets are organized as follows :

$$\mathbf{F} = \begin{bmatrix} f_{db_{1,1}} & \cdots & f_{db_{1,n_{db}}} & f_{wl_{1,1}} & \cdots & f_{wl_{1,n_{wl}}} \\ \vdots & \ddots & \vdots & \vdots & \ddots & \vdots \\ f_{db_{n,1}} & \cdots & f_{db_{n,n_{db}}} & f_{wl_{n,1}} & \cdots & f_{wl_{n,n_{wl}}} \end{bmatrix} \quad (2.1)$$

$$\mathbf{G} = \begin{bmatrix} g_{bl_{1,1}} & \cdots & g_{bl_{1,n_{bl}}} \\ \vdots & \ddots & \vdots \\ g_{bl_{n,1}} & \cdots & g_{bl_{n,n_{bl}}} \end{bmatrix} \quad (2.2)$$

\mathbf{F} represents the model generated training sets for the validation data (dumbbell (f_{db}) and three-leg wavelet (f_{wl}) energy dissipations). \mathbf{G} represents the model generated training sets for the target application (three-leg shock (g_{bl}) energy dissipations). The number of force levels at which energy dissipation is calculated (i.e. number of columns) for the corresponding configurations are denoted n_{db} , n_{wl} , and n_{bl} . For the present case, $n_{db}, n_{wl}, n_{bl} = 31$. There is no requirement that these three numbers be the same. The number of Iwan parameter sets is denoted n . Each row of \mathbf{F} and \mathbf{G} provides energy dissipation for each of these parameter sets and there must be a one-to-one correspondence within and between the rows of Eqs. 2.1 and 2.2. For the present case, $n = 20$.

The regression used is of the form

$$[\mathbf{1} \quad \mathbf{f}] \boldsymbol{\beta} = \mathbf{g} \quad (2.3)$$

where $\boldsymbol{\beta}$ is a $(1 + n_{db} + n_{wl})$ by n_{bl} matrix of regression coefficients. The vector \mathbf{f} is a $(n_{db} + n_{wl})$ by 1 row vector of energy dissipations for the dumbbell and the three-leg wavelet configurations, and the vector \mathbf{g} is a n_{bl} by 1 row vector of corrected three-leg shock energy dissipations. The $\mathbf{1}$ in the leading matrix of Eq. 2.3 allows for a constant offset to be estimated between the linear combination of dumbbell and three-leg wavelet dissipations, and the predicted three-leg shock dissipations. Equation 2.3 is regressed to the data provided by Eqs. 2.1 and 2.2. Specifically, $\boldsymbol{\beta}$ is estimated to satisfy Eq. 2.4 in a partial least squares (PLS) regression sense.

$$[\mathbf{1} \quad \mathbf{F}] \boldsymbol{\beta} \cong \mathbf{G} \quad (2.4)$$

The $\mathbf{1}$ correspond to a column vector of ones with the number of rows equal to the number of rows in \mathbf{F} .

The MATLAB function *plsregress* [8] was used to obtain a PLS estimate for $\boldsymbol{\beta}$ [9]. To address ill-conditioning or singular systems, PLS regression develops an intermediate space that's defined by \mathbf{F} and \mathbf{G} in terms of n_l latent components where n_l is specified by the user. Too few latent components results in a poor representation of \mathbf{F} and \mathbf{G} while too many latent components results in over-fitting of \mathbf{G} , leading to increased sensitivity of the regression to noise or error when applied to data other than the training sets. Unlike standard least squares regression and principal component analysis, PLSR is designed to address error in both \mathbf{G} and \mathbf{F} . Note that since models are approximations, we expect errors (differences from the actual energy dissipations for the systems modeled) in both \mathbf{F} and \mathbf{G} .

2.3.2 Choice of the Number of Latent Components

For the present analysis, the number of latent components chosen is based on the estimated prediction uncertainty of the regression model due to two sources of errors:

1. The errors in the ability of the regression model to represent the experimental data, and the projection of an estimate of these errors to the target application. These errors represent a model form error between the model as characterized by the training sets \mathbf{F} and the experimental observations \mathbf{y} ; and the additional model form error due to the regression. We estimate these errors through the residuals between the regression and the mean experimental observation for the dumbbell and three-leg wavelet experiment.
2. The errors in the ability of the regression model to represent \mathbf{G} . These errors are characterized by the residuals between the left and right sides of Eq. 2.4 across all training samples.

We assume independence between these two errors and sum the variance matrices to obtain a total that will be used to evaluate the number of latent components.

$$\mathbf{V}_1 = \mathbf{V}_{p,y} + \mathbf{V}_{regr} \quad (2.5)$$

The first term on the right corresponds to the variance in the projection of the model form error (item 1), and the second term on the right corresponds to the regression error (item 2). As will be illustrated later, the estimated variances depend on the number of latent components used for the regression.

Given a choice of the number of latent components n_l , the MATLAB function *plsregress* is used to evaluate the regression coefficients $\boldsymbol{\beta}$ of Eq. 2.4. MATLAB also returns a weighting matrix \mathbf{W} that specifies the weights used to map \mathbf{F} into the latent components. Specifically,

$$(\mathbf{F} - \mathbf{F}_\mu) \mathbf{W} = \mathbf{F}_s \quad (2.6)$$

where \mathbf{W} is a $(n_{db} + n_{wl})$ by n_l matrix. \mathbf{F}_μ contains the column-by-column means of \mathbf{F} (all rows of \mathbf{F}_μ are identical). We can think of the \mathbf{W} as the weights on the mean shifted \mathbf{F} that results in the n_l latent components that best represent the response space \mathbf{G} . Using this matrix to project the measurements into the latent component space gives

$$(\mathbf{y}_\mu - \mathbf{f}_\mu) \mathbf{W} = \mathbf{y}_s \quad (2.7)$$

\mathbf{y}_μ is a $(n_{db} + n_{wl})$ by 1 row vector of the mean measurements, \mathbf{f}_μ is vector comprised of the column means of \mathbf{F} (i.e., any row of \mathbf{F}_μ), and \mathbf{y}_s is a vector of the mapped mean measurements into the space of the latent components. Mapping the \mathbf{y}_s back into the measurement space gives

$$(\mathbf{y}_\mu - \mathbf{f}_\mu)_s = \mathbf{y}_s \mathbf{W}^{-1} \quad (2.8)$$

The residuals between the measurements, and the projected measurements mapped back into the measurement space, indicates how well the regression model can represent the experimental data. These residuals are

$$\mathbf{r} = (\mathbf{y}_\mu - \mathbf{f}_\mu) - (\mathbf{y}_\mu - \mathbf{f}_\mu)_s \quad (2.9)$$

The estimate of the variance of these residuals is

$$\sigma_r^2 = \frac{\mathbf{r} \mathbf{r}^T}{n_{db} + n_{wl} - 1} \quad (2.10)$$

The projection of this variance to the application conditions can be accomplished using the estimated regression matrix $\boldsymbol{\beta}$.

$$\mathbf{V}_{p,y} = \sigma_r^2 \boldsymbol{\beta}(2 : \text{end}, :)^T \boldsymbol{\beta}(2 : \text{end}, :) \quad (2.11)$$

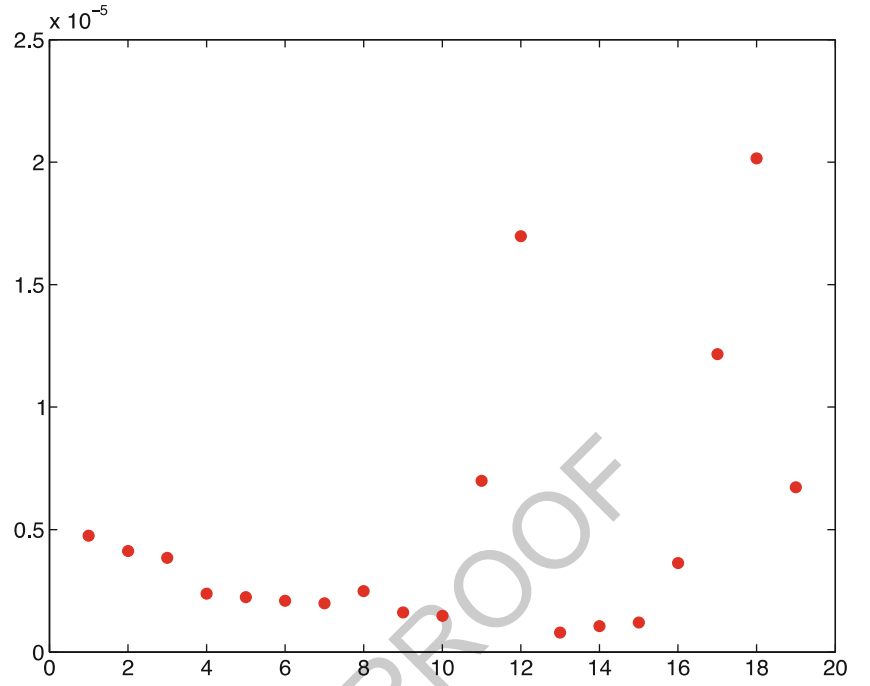
Note that the bias represented by the first row of $\boldsymbol{\beta}$ are not used.

The second source of error is that associated with the regression error on \mathbf{G} (see item 2 above). This can be estimated using the residuals between the left and right sides of Eq. 2.4.

$$\mathbf{V}_{regr} = \text{Var}(\mathbf{G} - [\mathbf{1} \ \mathbf{F}] \boldsymbol{\beta}) \quad (2.12)$$

Figure 2.6 illustrates the resulting sum of the diagonal elements of \mathbf{V}_1 (Eq. 2.5) as a function of the number of latent components. Note that there is a general increase in ability for the latent components to represent the data and the training set

Fig. 2.6 Regression quality and the number of latent components. $n_l = 10$ utilized for the remainder of the analysis



G, until n_l exceeds 10. At this point, the sensitivity of the regression to error between the mean validation data and the PLS representation overwhelms the benefit of using additional latent components. Based on these results, we will use $n_l = 10$ for the remainder of the analysis.

2.3.3 Unit-to-Unit Variability

Unit-to-unit variability is thought to be the dominant source of variability in the energy dissipation for the jointed structures of interest. As a result, the experiments were specifically designed to measure this variability, and the joint parameter sets for the model predictions were selected to represent this variability. As discussed earlier, data was collected from 45 realizations of the dumbbell tests, and 27 realizations of the three-leg tests under wavelet input conditions. Note that 27 realizations of the three-leg tests under shock conditions were also measured. These data are not used to develop the roll-up regression since such data would not be available for a prediction.

For the present analysis, we wish to correct not only mean behavior of the model for the target application using experimental data from the validation experiments, but also use this data to correct the unit-to-unit variability for the target conditions. Because the dumbbell experiments can be considered independent from the three-leg wavelet experiments, the variance matrix for the combined validation data can be written in block diagonal form as

$$\mathbf{V}_\gamma = \begin{bmatrix} \mathbf{V}_{\gamma,db} & 0 \\ 0 & \mathbf{V}_{\gamma,wl} \end{bmatrix} \quad (2.13)$$

where $\mathbf{V}_{\gamma,db}$ and $\mathbf{V}_{\gamma,wl}$ are the estimated variance matrices for the dumbbell and wavelet data. The projection of this unit-to-unit variability to the target application through the regression model is given by

$$\mathbf{V}_2 = \beta(2 : \text{end}, :)^T \mathbf{V}_\gamma \beta(2 : \text{end}, :) \quad (2.14)$$

Adding this unit-to-unit variability to the variability discussed earlier results in an estimated total uncertainty in the roll-up due to regression, observed differences between the regression model and the data, and due to unit-to-unit variability.

$$\mathbf{V}_{tot} = \mathbf{V}_1 + \mathbf{V}_2 \quad (2.15)$$

2.3.4 Bias and Uncertainty in the Simulation and Corrected Simulation Results

193

The large quantity of experimental data coupled with the multiple realizations associated with the training sets allows one to develop sampled based estimates of model bias, and uncertainty in bias. For the case of the model, there are 20 realizations of the model for each of the dumbbell, three-leg wavelet, and three-leg shock cases. As noted earlier, there are 45 realizations of the experimental data for the dumbbell, 27 for the three-leg wavelet, and 27 for the three-leg shock cases. Because, we do not know which model realizations (or joint parameters) are coupled with which sets of experimental data, we consider the experiments and the joint parameters realizations to be independent. We can have thus have 20×45 possible combinations of differences between the dumbbell experiments and model predictions, and 20×27 differences for each of the wavelet and shock configurations. For the case of the regression where both the dumbbell and wavelet results are used to estimate the shock experiment corrections, the number of differences increases significantly. For roll-up, there are 45×27 possible combinations of the dumbbell/wavelet experimental results, coupled with 20×20 possible combinations of the corresponding model results, resulting in $45 \times 27 \times 20 \times 20$ possible overall combinations. Rather than considering all of these combinations, we randomly sampled 2,000 subsets from each with replacement, and estimated the bias and uncertainty over the 2,000 samples for each force level. The results are presented in the following section.

2.3.5 Results

207

Figure 2.7 illustrates the results obtained by applying the process discussed in previous sections to the present application. The upper two plots indicate how well the PLS regression can represent the means of the experimental data, and the lower plot illustrates the corrected mean prediction for the target application. The experimental shock data for this target application was not used for the development of the regression, but is included as an indicator of the ability of the methodology to correct for model form error observed in the dumbbell and three-leg wavelet validation experiments. Plus and minus 2σ uncertainty bars are shown on the target application plot (twice the square root of the diagonal elements of Eq. 2.15). Note that the regression provides a good representation of the dumbbell and wavelet experiments. The regression also provides a somewhat improved representation of the shock prediction at higher shock force with little improvement at lower forces. Note that the dumbbell data lies within the range of the training set, whereas the wavelet data lies outside the range of the training set for forces greater than 275. The corrected model shows results that are outside the shock training set at forces greater than 290. The uncertainty in the corrected model at higher forces increases significantly, possibly reflecting the inability of the regression on the dumbbell and wavelet training sets to represent the shock model training sets at these forces. Overall, while the corrected model does not capture the actual experimental data for the shock experiments for all forces, the corrected model does represent an improvement over the uncorrected model results.

Figure 2.8 illustrates the results of using the sampling approach discussed previously. The top plot shows the experimental data and the model predictions (i.e. the training set) for the shock, whereas the bottom plot shows the corrected results using the regression. Note that the scatter in the training set for shock, is significantly less than that observed in the experimental data, whereas the scatter in the corrected realizations better match the scatter in the data for the largest forces. Because it is not clear to what extent this improved scatter is due of the observed behavior of the wavelet and dumbbell data, or due to the increased uncertainty in the ability to regress at high forces, caution must be exercised in interpreting these results.

Figure 2.9 shows an estimate of the model prediction bias and the uncertainty in this bias for the model results for all three cases, and also for the corrected model results for the shock. For this case, the sampling approach described above and the sampled results illustrated in Fig. 2.8 were used to estimate the 5, 50, and 95 % percentiles of the prediction to measured differences as a function of force. Note that the distributions are non-symmetric. Also note that the prediction error, as measured by the 50 %, and the corrected behavior at this percentile are similar at lower forces, but that the corrected model showed improved results at larger forces.

Overall, the corrected results provided an improved prediction of energy dissipation for the shock case, compared to the uncorrected results, over the range of the forces considered. However, based on the trend in the results illustrated in Fig. 2.7, the use of the corrected model results for input forces significantly larger than 350 will lead to an overcorrection in energy dissipation, illustrating the dangers of using a regression outside the range of the support provided by the experimental data.

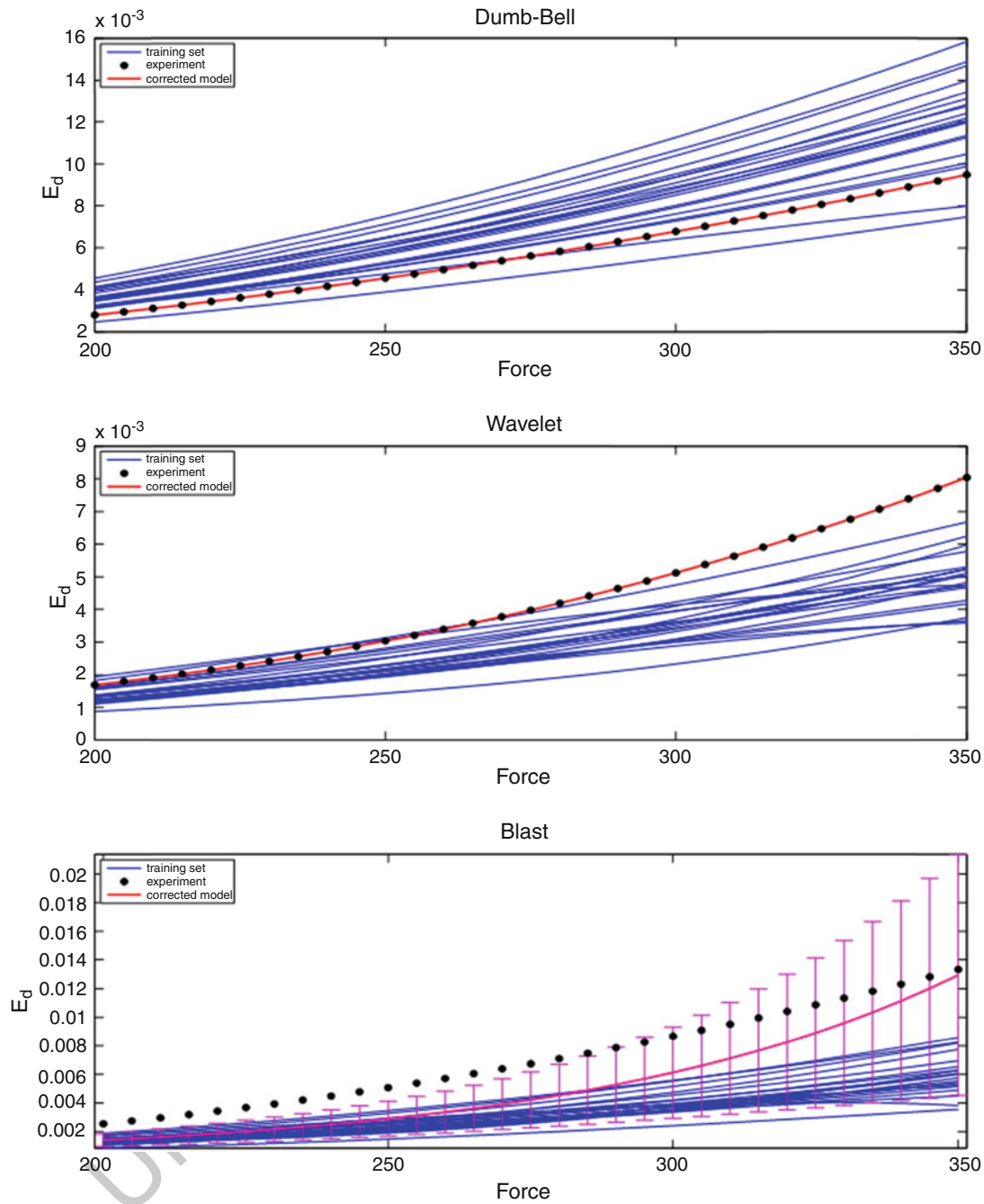


Fig. 2.7 Regression for mean validation data and corresponding correction for target application. Ten latent components are used

2.4 Summary

238

In this paper, we presented an approach to aggregate and extrapolation uncertainty information from component analysis to system level analysis. The approach develops a correction to model based predictions of energy dissipation for the three-leg configuration under shock loading, given the model predictions and experimental results for the dumbbell (Level 1) and three-leg wavelet test (Level 2) configurations. The Partial Least Squares Regression (PLS) based approach developed by Hills [7] is used to develop a linear relationship between differences in experiment and model predictions throughout a validation hierarchy, and a correction to a model prediction for the target application. Results presented in the paper are

239

240

241

242

243

244

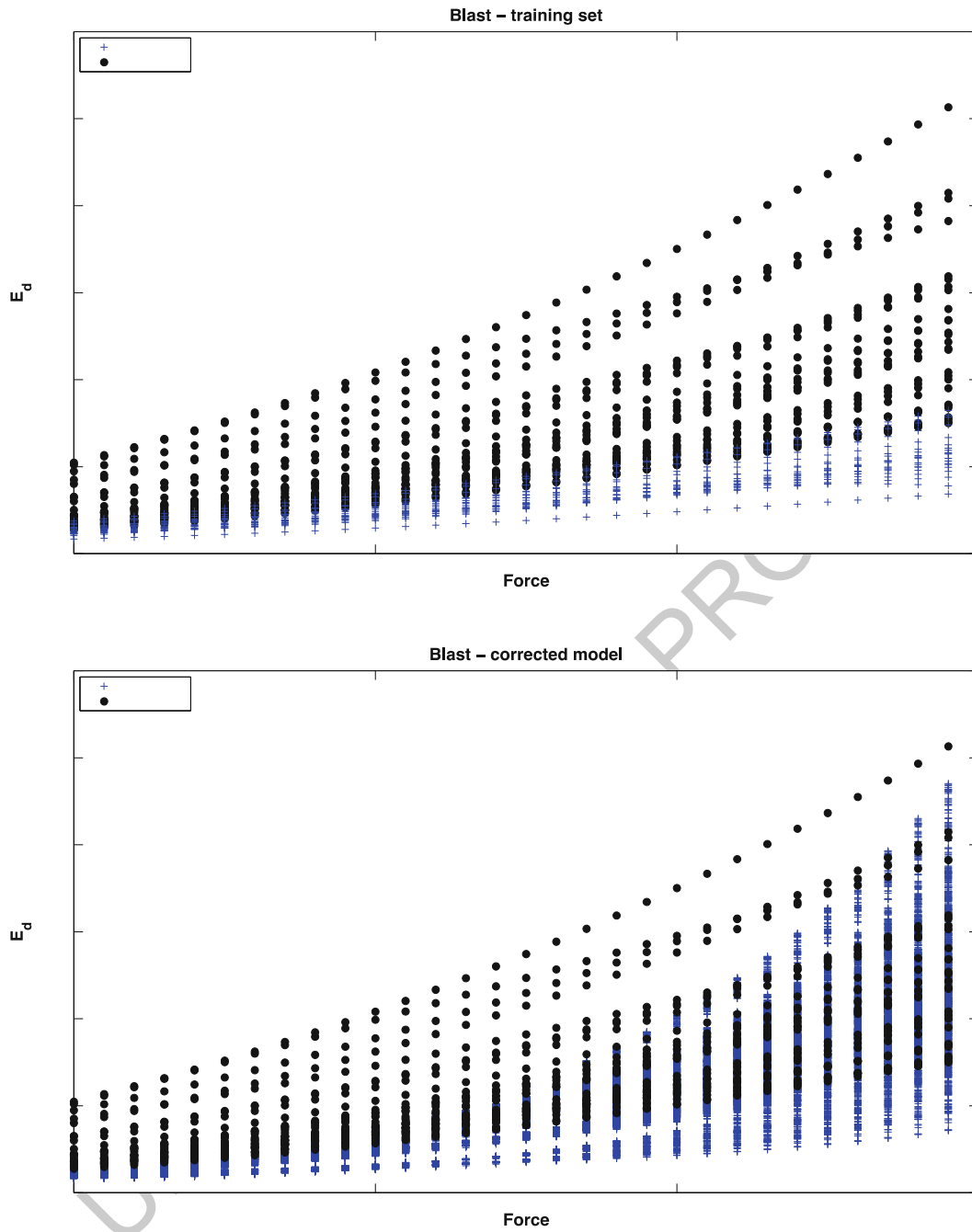


Fig. 2.8 Sampled results for the three-leg shock configuration (*black dots* represent experimental data and *blue+* represent model results—uncorrected in *top figure* and corrected in *bottom figure*)

encouraging when compared with actual measured data in the application space. It is noted in the paper that caution should be use when conducting large extrapolations outside the experimental data range.

Acknowledgments Sandia is a multi-program laboratory operated by Sandia Corporation, a Lockheed Martin Company, for the United States Department of Energy's National Nuclear Security Administration under Contract DE-AC04-94AL85000.

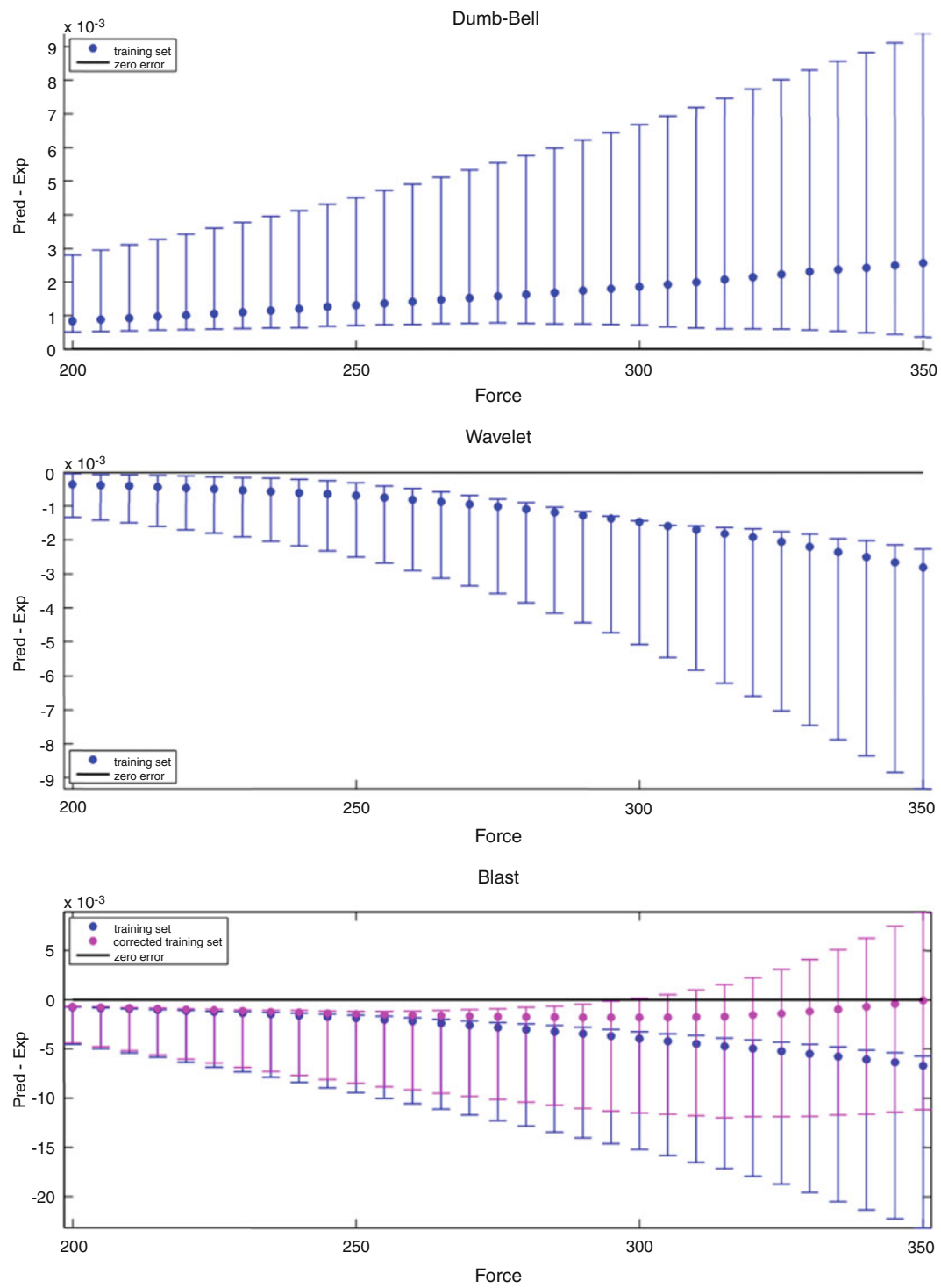


Fig. 2.9 Estimated CompSim uncertainty 5, 50, and 95 % percentiles for the three configurations

References

1. Oberkampf WL, Trucano TG (2000) Validation methodology in computational fluid dynamics, SAND 2000-1656C. Sandia National Laboratories, Albuquerque, NM 250
2. Sindir MM, Barson SL, Chan DC, Lin WH (1996) On the development and demonstration of a code validation process for industrial applications. 251
In: 27th AIAA fluid dynamics conference, AIAA Paper No. 96-2032, American Institute of Aeronautics and Astronautics, New Orleans, LA 253

3. Segalman D (2002) A four parameter Iwan model for lap-type joints, Sandia report, SAND2002-3828. Sandia Laboratories, Albuquerque, NM 254
4. Urbina A, Paez TL, Hasselman TK, Wathugala WG, Yap K (2003) Assessment of model accuracy relative to stochastic system behavior. In: 255
Proceedings of the 2003 AIAA/ASME/ASCE/AHS/ASC structures, structural dynamics, and materials conference 256
5. Reese G, Bhardwaj M, Segalman D, Alvin K, Driessen B, Pierson K, Walsh T (1999) Salinas—users notes, Sandia report 99-2801. Sandia 257
National Laboratories, Albuquerque, NM 258
6. Resor B, Gregory D (2006) Bolted joint experiments for structural dynamic model calibration and validation. In: Proceedings of the 24th IMAC 259
conference and exposition on structural dynamics, St. Louis, MO 260
7. Hill RG (2013) Roll-up of validation results to a target application, Sandia report SAND2013-7424. Sandia National Laboratories, Albuquerque, 261
NM, Sept 2013 262
8. MATLAB® Mathematics, Version 8, R2013a, The MathWorks, Inc., Natick, MA 263
9. de Jong S (1993) SIMPLS: an alternative approach to partial least squares regression. Chemomet Intell Lab Syst 18:251–263 264

UNCORRECTED PROOF

AUTHOR QUERY

AQ1. The bold variables are not clear and have been retained as per manuscript. Please check

UNCORRECTED PROOF

Model Validation and Uncertainty Quantification,
Volume 3

Proceedings of the 32nd IMAC, A Conference and
Exposition on Structural Dynamics, 2014

Atamturktur, H.S.; Moaveni, B.; Papadimitriou, C.;
Schoenherr, T. (Eds.)

2014, IX, 427 p. 303 illus., 233 illus. in color., Hardcover
ISBN: 978-3-319-04551-1